Tellus (2005), 57A, 742–757
Printed in Singapore. All rights reserved

Copyright © Blackwell Munksgaard, 2005
TELLUS

The effects on oceanic planetary waves of coupling with an atmospheric energy balance model

By RICCARDO FARNETI* and PETER D. KILLWORTH, *Southampton Oceanography Centre, Southampton, UK*

(Manuscript received 27 August 2004; in final form 17 February 2005)

ABSTRACT

This paper shows the existence of a growing planetary-wave-like ocean mode, with a decadal period and growth rate, which appears when a stratified, diffusive ocean is coupled to a simple atmosphere via an energy balance model (EBM). Such modes are not found when simpler surface ocean conditions are applied. The mode is low order in the vertical and, because of its slow growth, is likely to be observed in Earth System Models using an EBM in place of a fuller set of atmospheric dynamics. There is no apparent physical energy source for such a mode, and therefore it should not be expected to arise in such a model. The mode is analysed through a hierarchy of simple models, which differ only through their surface boundary condition.

1. Introduction

Energy balance models (EBMs) have been very useful for the development of coupled models for thermohaline circulation studies (Pierce et al., 1996; Bjornsson et al., 1997; Huck et al., 2001; Kravtsov and Dewar, 2003) as well as for decadal–interdecadal climate variability identification (Barsugli and Battisti 1998, hereafter BB98). The latter study found that the coupling of a simple ocean with an atmospheric EBM is able to reduce the energy fluxes between the ocean and atmosphere, increasing at the same time the variance of both the atmosphere and the ocean. It is argued in their paper that this model based on thermal coupling only is a valid tool for understanding the basic effects of ocean–atmosphere coupling at mid-latitudes. EBMs have also played a fundamental role in the early development of Earth System Models (North, 1975; North et al., 1981; Harvey, 1988; Trenberth, 1992; Weaver et al., 2001) because a fully active atmospheric model is usually too slow for the lengthy integration periods under investigation.

Although still very simplified, the one-dimensional EBM is very popular for reproducing coupled ocean–atmosphere systems (Kiehl, 1992). It is the simplest model of the coupled system at mid-latitudes and often agrees well with more sophisticated GCM studies. Other studies have focused on couplings with different oceans, from a slab ocean to an oceanic GCM, with sometimes the explicitly inclusion of the results of latent heat through moisture (Fanning and Weaver, 1996; Bjornsson et al., 1997).

None the less, EBMs are a drastic simplification of the atmospheric reality, and it is important to understand both their features and their shortcomings. Is it possible for a model including an EBM to possess unphysical responses, for example? A possible hint is given by the study by Goodman and Marshall (1999), who described a model which, using both dynamical and thermal forcing as coupling mechanisms, supports growing coupled modes in the decadal period via positive feedbacks between the atmosphere and the ocean. Some limitations of Goodman and Marshall (1999) were addressed by Ferreira et al. (2001), mainly in the use of a bounded basin, exploring the air–sea interactions at mid-latitudes with a two-layer quasi-geostrophic channel atmosphere. In their work, the atmosphere component of the coupled model consists of an EBM, similar to BB98, and explicit dynamics. When Ferreira et al. (2001) couple their atmosphere to an oceanic mixed layer, their results are in better agreement with previous GCM studies, with their success attributed to the inclusion of atmospheric dynamics.

The purpose of this paper is to examine how an EBM may be implicated in the production of a growing mode of oscillation when an EBM is coupled to an ocean under conditions relevant to climate simulations (long period, predominantly geostrophic, etc.). This is done by coupling a stratified ocean which includes a vertical diffusivity[1] to a succession of slightly more

*Corresponding author.
e-mail: ric01@noc.soton.ac.uk

[1]Qiu et al. (1997) have examined the effects of horizontal eddy diffusion in a 1.5-layer model, finding no change to the westward phase speed of free long baroclinic waves.

complicated surface boundary conditions, in the context of Rossby, or planetary, waves. These waves are the main mechanism whereby climatic information is carried around the ocean.

The concept of Rossby wave coupling to the overlying atmosphere is hardly new (consider White et al., 1998; White, 2000, for example), but no clear attempt has been made so far to explain or study the effects on the wave structure and propagation. None the less, experiments with coupled atmosphere–ocean systems in which planetary waves play a major role have proliferated (Frankignoul et al., 1997; Jin, 1997; Qiu and Jin, 1997; Goodman and Marshall, 1999; Colin de Verdière and Blanc, 2001; Ferreira et al., 2001) in the attempt of better understanding and increasing the predictability of the decadal–interdecadal climate variability.

Indeed, Jin (1997) found a spectral peak in the decadal–interdecadal period due to the resonance of the forced oceanic Rossby waves in his reduced-gravity uncoupled model, but also an oscillatory mode with an interdecadal peak when the model was coupled. Also, this mode was found to be unstable when positive thermal feedbacks were present.

The question of why planetary waves are observed to propagate faster than the linear theory predicts has been tackled in many ways. Since Chelton and Schlax (1996) published their results, many authors have tried to match the satellite results with a more complete theory. The inclusion of a baroclinic mean flow into a continuously stratified ocean, inducing changes in the gradient of potential vorticity, has been the first and probably the most successful study (Killworth et al., 1997). The results matched and explained the speed up of the waves and were in good agreement with observations almost everywhere. Although these results were a good approximation to the observed phase speeds, not all discrepancies were explained.

The importance of topographic effects was also considered in Killworth and Blundell (1999), but they were found to be negligible over an entire basin; however, when the effects of a mean flow and bottom topography are combined a second speed up is found (Killworth and Blundell, 2003).

The first study to address the question of how dissipative mechanisms influence the propagation of baroclinic planetary waves was by Qiu et al. (1997). Dissipation in the form of horizontal eddy diffusion in a 1.5-layer model of a forced ocean induced no changes in the westward phase speed of the free long baroclinic waves. Moreover, the free Rossby wave was found to be more sensitive to eddy dissipation at higher latitudes, due to its e-folding latitudinal dependence.

The purpose of this study is to identify another potential cause of differences in planetary wave propagation from the classic linear theory: the coupling with the atmosphere.

We are concerned not with direct wind or buoyancy forcing, which can be effective generators of forced waves, but with the response of the ocean surface to the atmosphere above for free waves.

We examine the role of an EBM as follows. After the introduction of the vertical diffusion coefficient K_v into the stratified ocean wave equation, exchanges with the atmosphere take the form of a surface boundary condition to an eigenmodal problem. Only the first few normal modes of the system are of interest, as the remainder possess higher vertical structure than is observed. Various boundary conditions will be employed: no flux to the atmosphere (NF, hereafter), a vertical diffusive heat flux of sensible heat to the atmosphere (HF, hereafter) and the coupling with an EBM. However, as we shall show, when an EBM provides a surface condition, a growing mode which is low order in the vertical is permitted. This mode does not exist with the other surface boundary conditions. More complete models involving an atmospheric EBM have proved the presence of sustained oscillations in the ocean (Cessi, 2000; Huck et al., 2001), but the inclusion of wind stress in the case of Cessi (2000) and of mean flow in Huck et al. (2001) was essential.

In Section 2 we set up the suite of problems, and in Section 3 we present the results. In Section 4 we examine the growing mode itself, and in Section 5 we discuss the implications for the use of EBMs in simple climate models.

2. Formulation of the coupling

2.1. The ocean

The introduction of the vertical diffusivity coefficient K_v into the long wave equations for a continuously stratified Boussinesq ocean on a β-plane is formulated.

The perturbation equations of momentum, continuity and conservation are

$$u_t - fv + \frac{1}{\rho_0} p_x = 0 \tag{1}$$

$$v_t + fu + \frac{1}{\rho_0} p_y = 0 \tag{2}$$

$$p_z = -\rho g \tag{3}$$

$$u_x + v_y + w_z = 0 \tag{4}$$

$$\rho_t + \bar{\rho}_z w = K_v \rho_{zz} \tag{5}$$

where u, v and w are the velocity components, ρ and p are the perturbation density and pressure fields, g is the gravitational acceleration, $f = f_0 + \beta y$ is the Coriolis parameter, β is the meridional gradient of f, K_v is the vertical diffusion coefficient and subscripts denote partial derivatives.

The addition of vertical diffusion effects requires some background density forcing to maintain the background stratification (which is denoted by an overbar). As is customary in perturbation studies, this is ignored henceforth.

Eliminating the vorticity terms between eqs. (1) and (2) we obtain

$$w_{ztt} + f^2 w_z - f\beta v - \beta u_t = \frac{1}{\rho_0} \nabla^2 p_t. \tag{6}$$

Introducing plane wave form eigensolutions of the type

$$[u, v, w, p] = \mathrm{e}^{\mathrm{i}(kx+ly-\sigma t)}[\hat{u}, \hat{v}, \hat{w}, \hat{p}]$$

and after using eq. (3), we have (dropping the hats)

$$f^2 w_{zz} - f\beta v_z + \mathrm{i}\sigma\beta u_z = \frac{-\mathrm{i}\sigma(k^2+l^2)}{\rho_\mathrm{o}}\rho g. \tag{7}$$

Here we have made use of the approximation of low-frequency motions, $\sigma \ll |f|$, typical for planetary wave studies.

To leading order we may now substitute geostrophy

$$u = \frac{-\mathrm{i}lp}{f\rho_\mathrm{o}}, \qquad v = \frac{\mathrm{i}kp}{f\rho_\mathrm{o}}$$

into eq. (7), arriving at the expression

$$f^2 w_{zz} + \beta\mathrm{i}k\frac{\rho g}{\rho_\mathrm{o}} = -\mathrm{i}\sigma(k^2+l^2)\frac{\rho g}{\rho_\mathrm{o}}, \tag{8}$$

where again $\sigma/f \ll 1$ has been used. This leads in turn to

$$\rho = \frac{\mathrm{i}f^2\rho_\mathrm{o}}{g[\sigma(k^2+l^2)+\beta k]} w_{zz}, \tag{9}$$

which relates the density to the second derivative of w. This relationship will be used throughout this study to formulate the coupling as one of the boundary conditions at the surface.

Substituting the expression for ρ into the conservation of density and rearranging yields an expression for the vertical velocity

$$N^2[\sigma(k^2+l^2)+\beta k]w = -\mathrm{i}K_\mathrm{v} f^2 w_{zzzz} + \sigma f^2 w_{zz}, \tag{10}$$

where $N^2 = -g\bar{\rho}_z/\rho_\mathrm{o}$.

Diffusion, being a fourth derivative, is therefore not expected to alter the frequency of the wave significantly. In fact, the surface boundary layer generated by K_v should have a thickness of 100–200 m depending on k (this is discussed later). Computing the phase speeds with the inclusion of the predicted homogeneous boundary layer leads to no differences from the unperturbed solutions.

Setting $K_\mathrm{v} = 0$ reduces the problem to the classical Sturm–Liouville problem (e.g. Gill, 1982)

$$w_{zz} + \frac{N^2}{C^2} w = 0 \tag{11}$$

together with vanishing w at surface[2] and floor, where the eigenvalue C, the internal wave speed, is related to the frequency by

$$\sigma = -\frac{\beta k}{(k^2+l^2)+a^{-2}} \tag{12}$$

and $a = C/f$ is the Rossby radius of deformation.

If the diffusivity is non-zero, then two more boundary conditions are required for the fourth-order eigenvalue problem (10). The condition of no heat flux through the floor requires from eq. (9) that

$$w_{zzz} = 0, \qquad z = -H. \tag{13}$$

The last boundary condition is at the surface. In the case of no heat flux at the surface (the NF case), eq. (9) gives

$$w_{zzz} = 0, \qquad z = 0, \tag{14}$$

although this boundary condition will be changed later to permit fluxes to and from the atmosphere.

The eigenvalue problem (10), (13), (14) must be solved numerically (although analytical solutions are possible for simple forms of $N^2(z)$, the algebra is tedious and unenlightening). The problem is cast on to a fine-resolution finite-difference grid (5-m spacing) so that any boundary layer structure can be adequately resolved. Such resolution is not too computationally expensive. Then, eq. (10) is converted into a matrix eigenvalue problem of the form $\mathsf{A}\hat{w} = \sigma\mathsf{B}\hat{w}$, where A and B are the matrices of the coefficients and $\sigma = (\sigma_r + \mathrm{i}\sigma_i)$ the complex eigenfrequency; the eigenvectors $\hat{w}$ and associated eigenvalues are ordered by decreasing value of σ. The meridional wavenumber, l, is set to zero for simplicity. The square of the Brunt–Väisälä frequency, N^2, is an exponential function of z ($N^2 = N_0^2\mathrm{e}^{-\gamma z/H}$), where $N_0^2 = 10^{-5}\,\mathrm{s}^{-2}$ is the stratification at $z = 0$ and $\gamma = 3.7$ a typical mid-latitude value (Killworth et al., 1997).

The system is solved numerically with NAGLIB's generalized eigenvalue problem solver routines.

With a β-plane centred at 30°N, we set

$$f = 0.7 \times 10^{-4}\,\mathrm{s}^{-1}, \qquad \beta = 2 \times 10^{-11}\,(\mathrm{m\,s})^{-1},$$

$$K_\mathrm{v} = 10^{-4}\,\mathrm{m}^2\,\mathrm{s}^{-1}, \qquad H = 5 \times 10^3\,\mathrm{m}.$$

For the stratification considered, $C_1 = 2.377\,82\ \mathrm{m\,s}^{-1}$ is the internal wave speed for the first mode, and therefore $a = C_1/f = 23.7782 \times 10^3$ m is the Rossby radius of deformation. Due to the choice of a weak N_0^2, the resulting radius of deformation is possibly small, but the effects on the eigenmodes will be discussed later.

2.2. Atmospheric energy balance model

A one-dimensional, linear EBM is used to simulate the basic coupling between the atmosphere and ocean in the mid-latitudes.

We use here the model of BB98 with the only difference being that there is no dynamical forcing in this case. The basic mechanisms of the different EBMs in the literature are very similar. The model takes into account the balance between short-wave, long-wave and surface fluxes and thus reproduces the balance of incoming and outgoing radiant energy. The equations of BB98, linearized about the climatological mean state and neglecting any dynamical forcing, are

$$\gamma_\mathrm{a}\partial_t T_\mathrm{a} = -\lambda_\mathrm{sa}(T_\mathrm{a} - T_\mathrm{o}) - \lambda_\mathrm{a} T_\mathrm{a} \tag{15}$$

[2]The assumption of a rigid lid does lose the possibility of an interaction between barotropic and baroclinic modes, which could occur in the presence of diffusion. This is likely to be negligible, because it is of the order of the small parameter C^2/gH.

$$\gamma_o \partial_t T_o = \lambda_{so}(T_a - T_o) - \lambda_o T_o. \quad (16)$$

Here, subscripts 'a' and 'o' refer to atmosphere and ocean, respectively; T is the anomalous temperature; $\gamma_a = \rho_a C_{pa} H_a$ and $\gamma_o = \rho_o C_{po} H_o$ are the heat capacities; λ_s is the linearized coefficient of combined latent, sensible and long-wave heat flux; λ_a and λ_o (bulk transfer coefficients) are the radiative damping of each component to space. The standard values for the ocean are $\rho_o = 1024$ kg m^{-3}, $C_{po} = 4 \times 10^3$ J (kg K)$^{-1}$, $T_o = 285$ K, and for the atmosphere $\rho_a = 1.25$ kg m^{-3}, $C_{pa} = 4 \times 10^3$ J (kg K)$^{-1}$, $T_a = 270$ K, $H_a = 8.4 \times 10^3$ m, $\epsilon = 0.76$, $\sigma_b = 5.67 \times 10^{-8}$ W(m^2 K^4)$^{-1}$, where ϵ is the long-wave emissivity and σ_b is the Stefan–Boltzmann constant. Finally, following BB98, we choose $\lambda_{sa} = 23.9$, $\lambda_{so} = 23.4$, $\lambda_a = 2.8$ and $\lambda_o = 1.9$ (in units of W m^{-2} K^{-1}).

After taking the Fourier transform ($\partial_t \rightarrow -\mathrm{i}\sigma$), the equations of BB98 take the form

$$-\mathrm{i}\sigma \gamma_a T_a = \lambda_{sa} T_o - (\lambda_{sa} + \lambda_a) T_a \quad (17)$$

$$-\gamma_o' K_v \partial_z T_o = \lambda_{so} T_a - (\lambda_{so} + \lambda_o) T_o. \quad (18)$$

Here, the ocean heat equation has been converted into a vertical diffusive flux towards the interior, the ocean heat capacity has become $\gamma_o' = \rho_o C_{po}$ and the assumption that

$$\rho_o C_{po} K_v \partial_z T_o \cong \rho_o C_{po} H_o \partial_t T_o, \quad (19)$$

where H_o is a mixed layer depth, has been made.

The ocean eq. (18) is the same as that used in Bjornsson et al. (1997), see their eq. (20), if the contribution from the evaporation term is neglected.

It is straightforward to prove that eqs. (17) and (18), with eq. (19) substituted, is a stable system with two different and negative eigenvalues.

From eq. (17)

$$T_a \left(\frac{\lambda_{sa} + \lambda_a}{\lambda_{sa}} - \mathrm{i}\sigma \frac{\gamma_a}{\lambda_{sa}} \right) = T_o, \quad (20)$$

which describes the relationship between the atmospheric and oceanic temperature for every eigenfrequency; the presence of an imaginary part indicates a phase shift between T_a and T_o.

Substituting eq. (20) into eq. (18) and rearranging yields

$$-\frac{\gamma_o'}{\lambda_{so}} K_v \partial_z T_o = \left(\frac{\lambda_{sa} + \lambda_a}{\lambda_{sa}} - \mathrm{i}\sigma \frac{\gamma_a}{\lambda_{sa}} \right)^{-1} T_o - \left(\frac{\lambda_{so} + \lambda_o}{\lambda_{so}} \right) T_o, \quad (21)$$

or

$$-\Gamma_o' \partial_z T_o = \left[(\Lambda_a - \mathrm{i}\sigma \Gamma_a)^{-1} - \Lambda_o \right] T_o, \quad (22)$$

where the following substitutions have been made: $\Gamma_o' = (\gamma_o'/\lambda_{so}) K_v$, $\Gamma_a = (\gamma_a/\lambda_{sa})$, $\Lambda_o = (\lambda_{so} + \lambda_o)/\lambda_{so}$ and $\Lambda_a = (\lambda_{sa} + \lambda_a)/\lambda_{sa}$.

Equation (22) will be the new surface boundary condition for eq. (10) in the EBM case.

Using again the relationship described in eq. (9), the suitable form for the boundary condition in the EBM case becomes

$$-\Gamma_o' w_{zzz} = \left[(\Lambda_a - \mathrm{i}\sigma \Gamma_a)^{-1} - \Lambda_o \right] w_{zz}, \quad (23)$$

The accuracy of our grid spacing was tested for the resulting σ and the length-scale (of around 10 m) was found to be well resolved.

The new coupling involves incoming long-wave and surface fluxes to the ocean modulated by the eigenfrequency and a direct estimate of the atmospheric and oceanic temperature feedback.

2.3. A surface thermal boundary condition

To permit investigation of the possible effects of simpler matching to the atmosphere, we also construct a simpler coupling of heat fluxes at the ocean surface through a surface thermal boundary condition. Restoring boundary conditions implicitly model the atmosphere and the vertical diffusive heat flux only considers the sensible heat (Haney, 1971). In this case, only losses towards the atmosphere are possible.

In this case we allow a heat flux to the atmosphere with a simple matching via one of the boundary conditions. We consider a standard vertical diffusive heat flux

$$Q = -\rho_0 C_{po} K_v \partial_z T_o, \quad (24)$$

where

$$Q = \partial_T Q T',$$

is proportional to the vertical diffusivity of heat and the vertical gradient of temperature, C_{po} is the ocean heat capacity and T_o its temperature.

The heat flux Q is reformulated in order to give the following expression

$$-K_v \partial_z T_o|_{z=0} = \tau T', \quad (25)$$

where T' is the difference between oceanic and atmospheric temperature and $\tau = (1/\rho_0 C_{po})\, \partial_T Q = 1.15 \times 10^{-5}$ m s^{-1}, corresponds to the sensible heat and can be thought of as the restoring time-scale of a mixed layer relaxing to the prescribed temperature; for a mixed layer depth of 30 m, this time-scale would be of 30 d. The negative sign on the left-hand side (l.h.s.) of eq. (25) means a return towards zero of any surface perturbation temperature. Assuming that the perturbation densities are function of the perturbation temperatures only, $\rho' = -\alpha \rho_0 T'$, and using the relationship in eq. (9), eq. (13) is included as a surface boundary condition for eq. (10) and the top boundary condition for the third derivative in the HF case takes the form

$$w_{zzz} = -\mu w_{zz}, \quad (26)$$

where $\mu = \tau / K_v$. This would imply a length-scale $\mu^{-1} = K_v/\tau$, which for $K_v = 10^{-4}$ m^2 s^{-1} is equal to 10 m and therefore adequately resolved by our 5-m grid spacing. For a smaller diffusivity value, e.g. 10^{-5} m^2 s^{-1}, the length-scale would reduce

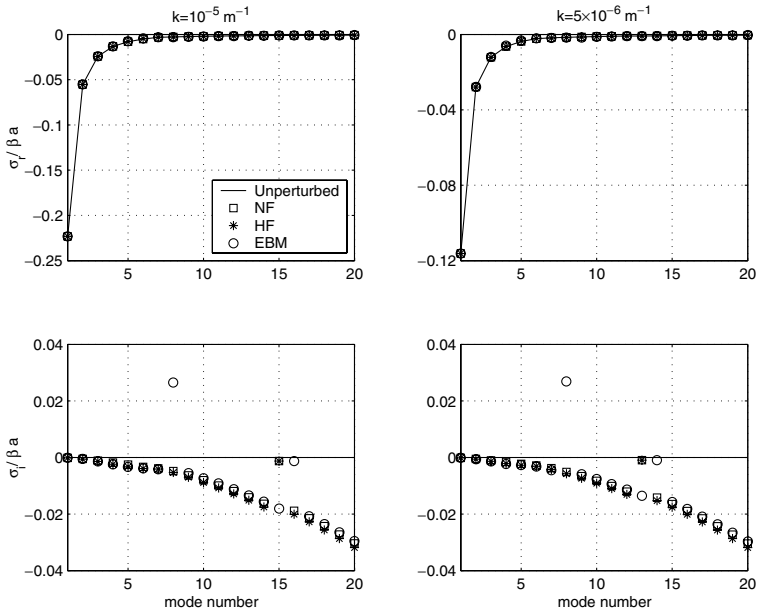

Fig. 1. Real and imaginary parts of the eigenfrequencies for $k = 10^{-5}$ m^{-1} and $k = 5 \times 10^{-6}$ m^{-1} (NF = no fluxes, HF = heat fluxes and EBM = energy balance model). No differences are found for Re(σ) and only small decays exist for Im(σ). Whilst all the modes resemble each other in the different cases, an unstable mode appears for the EBM and a slowly decaying one for the NF and HF cases as well.

to 1 m; however, the results have been tested with a 4-m and a 3-m spacing without changes in the solution.

3. Discussion

For selected wavenumbers, the real and imaginary parts of the eigenfrequencies resulted from the solution of the eigensystem (10)–(13)–(22) are plotted for the first 20 least damped modes in Fig. 1.

Re(σ) (top panels) is not noticeably perturbed by the coupling for any of the first 20 modes, but Im(σ) presents some peculiarities. Besides the intuitive increase in damping rate as we move to higher mode numbers, an unstable mode [Im(σ) > 0] and a slowly decaying mode are present for both selected wavelengths in the EBM case.

This is a surprising result, because an instability is not expected to rise from a thermal coupling of this kind and there is no apparent source of energy. Sensible heat exchanges with the atmosphere are expected to provide a sink of energy and therefore an extra damping to the diffusive ocean. Unstable coupled modes need a source from either the ocean or the atmospheric reservoir to release available potential energy. In our simple model there is no mean flow in the ocean or in the atmosphere and the coupling is given only by thermal exchanges. Mean flows and wind stress are essential factors for developing growing coupled modes through ocean–atmosphere positive feedbacks (Qiu et al., 1997; Goodman and Marshall, 1999; Cessi, 2000; Cessi and Paparella, 2001; Colin de Verdière and Blanc, 2001; Huck et al., 2001). In the model presented here there is no kinetic energy because the basic state is motionless and no available potential energy in either the ocean or the atmosphere, therefore there is no energy to sustain instabilities.

Interestingly, the slowly decaying mode found in Fig. 1 is present for the NF and HF cases as well, where only losses towards the atmosphere are present, but the growing mode appears only when the EBM is coupled to the ocean. Both Colin de Verdière and Huck (1999) and Huck and Vallis (2001) found interdecadal oscillations in their ocean forced by constant surface heat fluxes, but in our simple representation these are not supported under the HF case. However, we can speculate, as discussed later, that the weakly damped mode highlighted before might become unstable under more realistic physical conditions.

A global view of the main results is summarized in Fig. 2. Here, the dispersion relation for the first two baroclinic modes of the linear unperturbed theory is compared with the results from our three alternative surface conditions.

None of the simple couplings applied to the planetary wave changes its frequencies significantly, and therefore its phase velocities are essentially the same as the linear theory predicts. Some discrepancies from the standard linear theory appear only at very long wavelengths λ_w (around 10^7 m, much longer than any observed planetary wave) where greater decaying rates [Im(σ)] are found.

Decay rates are plotted in the bottom panel of Fig. 2. Here a slow increase in Im(σ) is clear as the wavenumber moves towards longer waves for all three cases. For long wavelengths, the EBM produces the strongest damping, although in a range of λ_w from decadal to annual period ($\lambda_w = 10^6$–10^4 m) the HF dominates. This was to a certain point predictable as the EBM includes some incoming fluxes that counteract the outgoing fluxes, also included in the HF case. Therefore, the first mode is weakly damped everywhere, whereas the second and successive modes are more and more damped. The result is then an insensitivity of

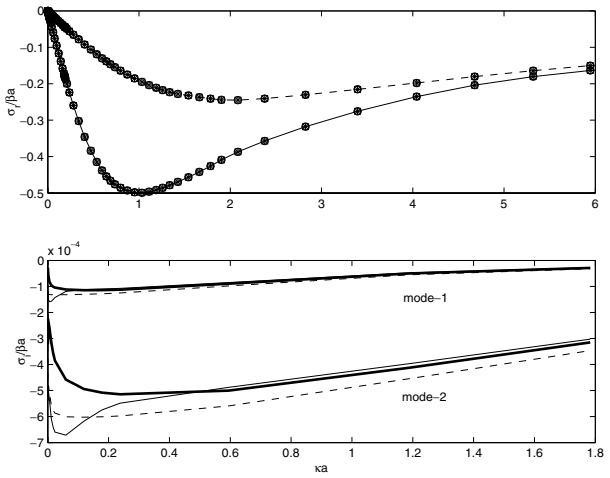

Fig. 2. Dispersion relation for the first and second modes for all three cases studied ($N_0^2 = 10^{-5}$ s^{-2}, $K_v = 10^{-4}$ m^2 s^{-1}). The frequency is scaled by $1/\beta a$ and the wavenumber by a. Top panel: real part of the frequency. Solid and dotted lines correspond to the unperturbed solution for the first and second modes, respectively. □ = diffusivity-only case (NF), ∗ = heat flux case (HF), ○ = EBM case. Bottom panel: decaying rate of the first and second modes for the three cases. Thick solid lines = NF, solid lines = HF, dashed line = EBM.

the first mode to all these couplings and a small dependence of the following ones.

The vertical structure of the wave is also analysed. The unperturbed non-diffusive solution, together with the results of the different surface conditions, is shown in Fig. 3 for the first three modes for the stratification considered. The eigenvectors are almost independent of the wavenumber but this is not the case when they become complex. For a wave with $\lambda_w = 6 \times 10^5$ m, vertical diffusivity only and the two couplings have negligible effects on the eigenstructure; when we move toward longer waves, the effects are visible from the third mode ($\lambda_w = 6 \times 10^6$ m, right panel of Fig. 3). As anticipated by the dispersion relationship, damping starts to be 'felt' at higher modes and longer waves.

After computing the solutions for all matchings and looking at different wavenumbers, neither a surface boundary layer nor any significant difference from the linear unperturbed vertical structure could be found in the first mode.

Moreover, no discernible difference was found in the perturbation of the vertical structure from the HF or the EBM coupling. The introduction of unrealistically high K_v (10^{-3} m^2 s^{-1}) into the wave equations is significant in the vertical structure in the second and higher modes, as can be seen for the NF case in Fig. 4. The dependence of the eigenfrequencies on changes in K_v showed similar results: the real part remains unaffected for all modes while σ_i starts to be perturbed by diffusivity from the second mode if $K_v = 10^{-3}$ m^2 s^{-1} as found for the vertical structure. Therefore, vertical diffusivity only and the coupling through heat fluxes do not slow down the wave or damp it effectively, even with unrealistically high values. This result is in contrast with previous studies, which suggested that planetary waves could be slowed and damped by Newtonian cooling by the atmosphere (White, 2000).

Sensible heat fluxes seem to be the most successful mechanism in damping out the wave; in the EBM, positive contributions of sensible and latent fluxes to the ocean do exist, possibly inducing some positive feedbacks that diminish the net loss to the atmosphere and therefore the damping of the wave.

Because more damping effects are found for the second mode, it is interesting to look at the whole spectrum of modes (Fig. 1).

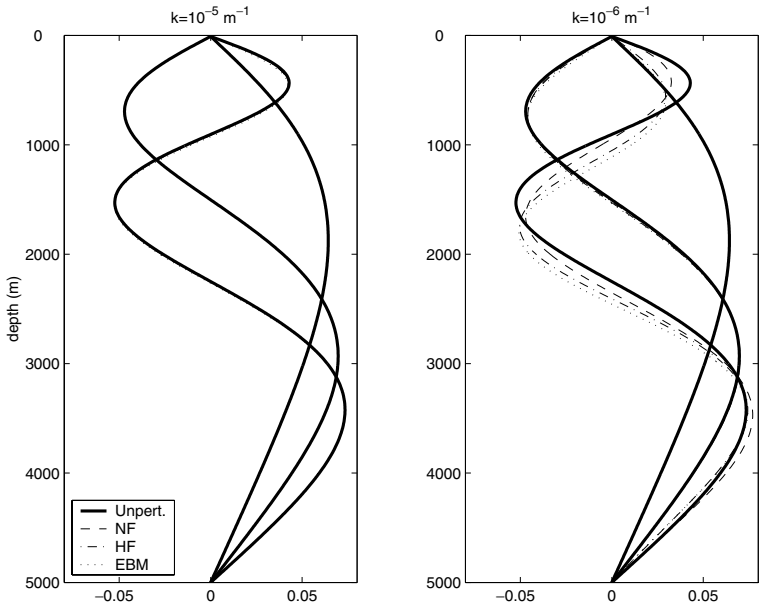

Fig. 3. Solutions for the vertical structures of the first three modes for the three cases. Only the third mode at long wavelengths starts being significantly modified.

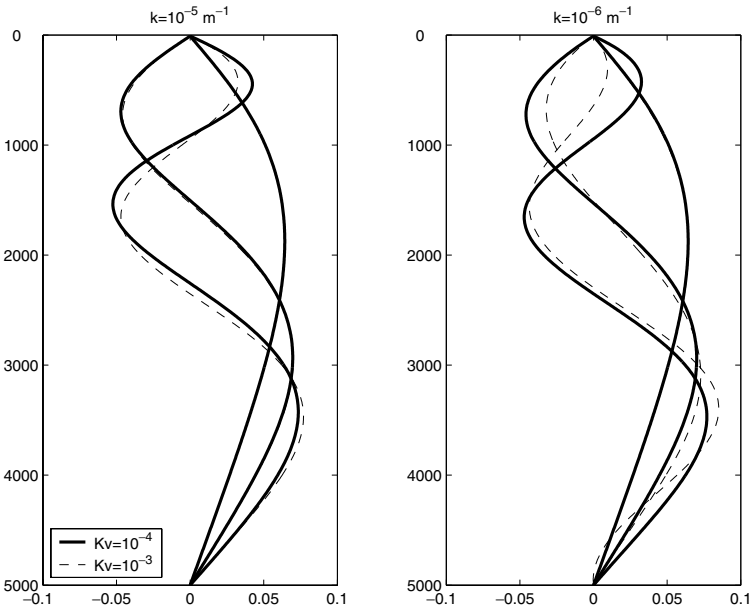

Fig. 4. Effects of changes in the diffusivity coefficient on the first three modes for selected wavenumbers in the NF case. When K_v is increased from 10^{-4} m^2 s^{-1} to 10^{-3} m^2 s^{-1}, the second mode, and for long waves also the third mode, is perturbed. Therefore, the K_v value necessary to modify the vertical structure is too high.

These are progressively slower and hence they have more time to interact with the overlying atmosphere and, in this case, be damped by heat losses.

Weakly dissipated modes have been recently discussed by Cessi and Primeau (2001). Within the free basin modes, they found the existence of weakly damped modes promoted by dissipation; moreover, these ocean-only modes can be excited by dynamical air–sea coupling (Cessi and Paparella, 2001). In fact, Jin (1997) discussed a coupled mode that under a moderate thermal damping was weakly damped but when positive coupled feedbacks are acting the mode turns out to be weakly unstable. Therefore, while the unstable modes generated by the EBM result from a different process, we hypothesize that the slowly decaying modes found with the NF and HF cases could be generated by similar mechanisms as those found by Cessi and Primeau (2001), and possibly become sustained by a subsequent atmospheric forcing.

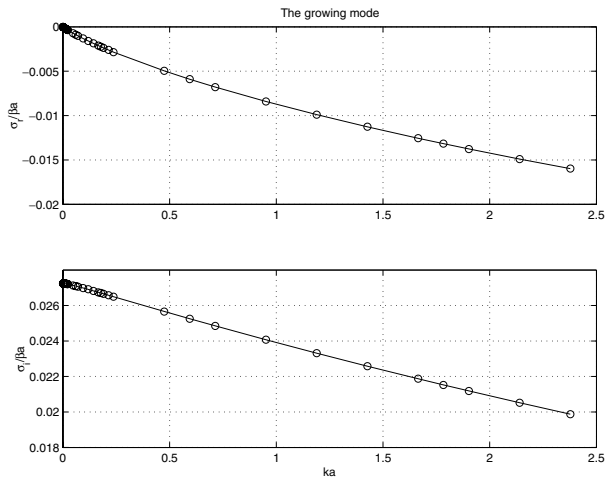

Fig. 5. Re(σ) and Im(σ) of the unstable mode for the long wave band.

4. Structure and growth of the unstable mode

The mode with a positive imaginary part found in Fig. 1, implying a growing disturbance, exists for a wide range of wavenumbers (Fig. 5), including the physically significant range. In the long-wave limit, the growth rate varies linearly with the wavelength. Its vertical structure resembles that of a first mode, becoming more oscillatory in the vertical as the wavelength decreases; this holds for its imaginary part as well, which is of the same order of magnitude as the real part (Fig. 6). Clearly, this mode arises from the interaction of the wave with the overlying EBM and its incoming energy; the longer the wave, the more it interacts with the atmosphere.

At the beginning of this paper we suggested the possibility of a boundary layer arising due to the inclusion of K_v and different matching at the surface, but this was not found for any of the modes. In contrast, this growing mode possesses a clear surface boundary layer (Fig. 6) which deepens as $k \to 0$. A preliminary study suggested that, with the introduction of K_v into the long-wave equations, the dependence of the boundary layer thickness δ on diffusivity would be described by

$$\delta \sim \frac{1}{a\sqrt{\beta}} \left(\frac{K_v}{k} \right)^{1/2}. \tag{27}$$

This would give a δ of about 200 m for $\lambda = 6 \times 10^6$ m, which is roughly what we obtain in the growing mode. Also, after computing the vertical structure for several k, it was observed that the decay of δ towards smaller wavelengths is linear and therefore contradicting the previous relationship. However, eq. (27) would describe a boundary layer for a no-heat-flux condition where eq. (14) holds; in this case, the EBM needs to be present for the

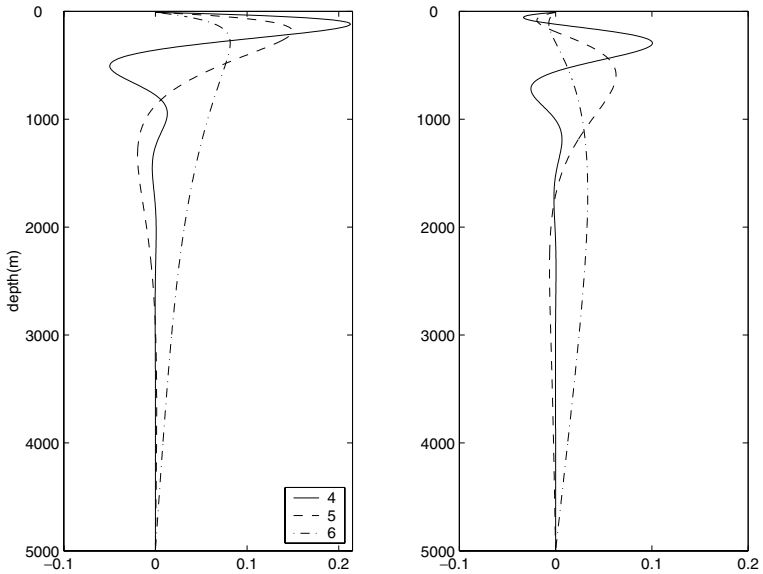

Fig. 6. Vertical structure of the growing mode. Re(w) (left panel) and Im(w) (right panel). Solutions are plotted for $k = 10^{-4}$, 10^{-5}, 10^{-6} m^{-1}. Note how the boundary layer thickness is linearly increasing with k.

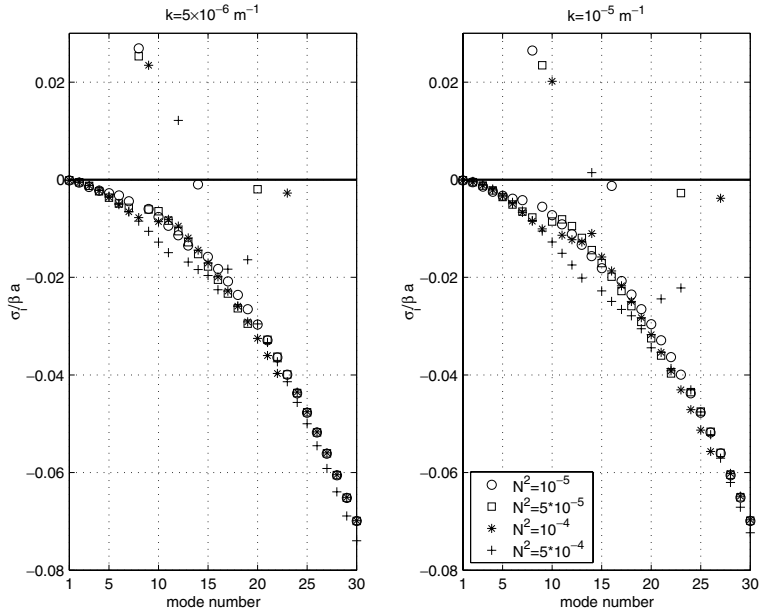

Fig. 7. Responses of the decaying rate to changes in N_0^2 (s^{-2}). As the exponential stratification increases, the unstable mode is displaced toward higher modes and its growth rate becomes smaller. The same is happening for the slowly decaying mode, which is approaching the other modes. Note how shorter waves are more sensitive to changes in N_0^2.

unstable mode to exist, and therefore the theoretical behaviour of δ is expected to be different from that found here.

The other singular mode, the slowly decaying mode, has a bottom trapped structure and no particular changes are found when the air–sea coefficient λ or K_v vary, as only the surface trapped growing mode will be sensitive to changes at the surface.

4.1. Parameter sensitivity

In order to understand the response of this unstable mode to changes in the background conditions, we carried out sensitivity analyses on the main parameters that could control the ocean–atmosphere interaction.

As the selected value for the stratification is slightly weak ($N_0^2 = 10^{-5}$ s^{-2}) we studied the eigenresponse to an increase in the ocean stratification. In Fig. 7 the decaying rates for different N_0^2 are plotted. The growing rate diminishes and the unstable mode is shifted towards higher modes, indicating that a lower frequency is needed to interact positively with the EBM. The same happens for the slowly decaying mode and for both wavenumbers ($k = 5 \times 10^{-6}$ m^{-1}, $k = 10^{-5}$ m^{-1}). At the same time, with stronger stratification the response is more concentrated in the surface layer and more oscillations in the vertical start to appear

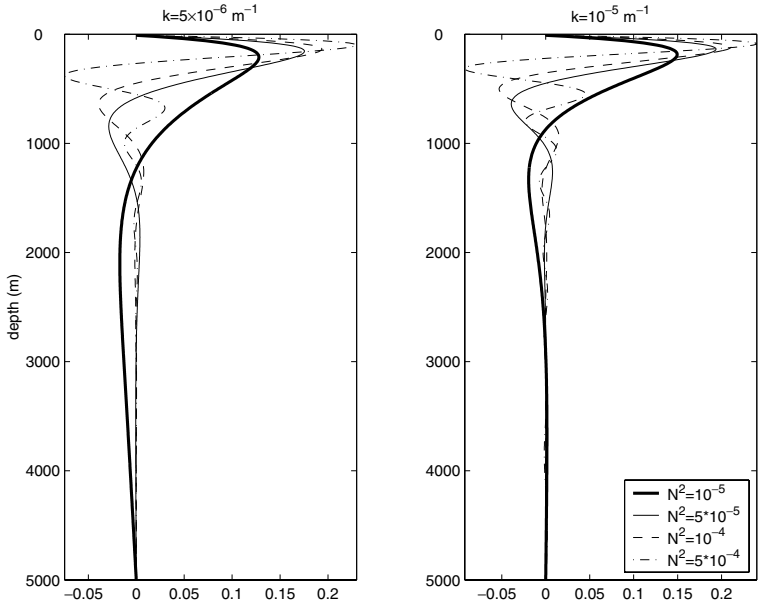

Fig. 8. Structure of the unstable mode at different stratifications (s^{-2}). With stronger N_0^2 the mode is trapped at the surface with more oscillations in the vertical.

(Fig. 8). Interestingly, surface intensified unstable modes have also been found by Huck et al. (2001) in their three-dimensional dynamical ocean model forced by constant surface fluxes. Their unstable mode, studied in the framework of quasi-geostrophic baroclinic instability and identified as potential vorticity waves (a kind of planetary waves), relied on the background flow in order to propagate. In our case such a mode could not exist, lacking our model of a circulation on which the unstable wave could grow.

In our study, with an exponential profile for the Brunt–Väisälä frequency, the mixed layer is not represented. Because the heat exchanges with the atmosphere are concentrated at the surface, the inclusion of a mixed layer could be important. Therefore, we studied the case of an exponentially stratified ocean with a homogeneous mixed layer at the top. In this case, we used the same exponential stratification $N^2 = N_0^2\, \mathrm{e}^{-\gamma z}$ (where again $N_0^2 = 10^{-5}\ \mathrm{s}^{-2}$ and $\gamma = 3.7$) and we introduced a homogeneous layer of different thickness δ at the surface, i.e.

$$N^2 = \begin{cases} 0, & -\delta \le z \le 0 \\ N_0^2 \mathrm{e}^{-\gamma z}, & -H \le z \le -\delta \end{cases} \tag{28}$$

Applying the same boundary conditions for the coupling and using values in the range $300 \le \delta \le 0$ m, no significant differences were found, apart from similar changes obtained when N_0^2 is modified (not shown). The unstable mode is still present, indicating that the heat exchanges at the surface are rapidly transmitted into the interior of the ocean and the homogeneous mixed layer is not able to modify the wave response. Also, introducing the homogeneous surface layer in the stratified ocean did not change the characteristics of the internal wave propagation, resulting in similar wave speeds and vertical structure.

Another fundamental parameter is the coefficient of air–sea exchange λ, which is included in λ_{sa}, λ_{so}.[3] An increase in λ would mean a stronger communication between the wave and the EBM leading to an excitement of the coupled unstable mode. This is clearly seen in Fig. 9 when λ is changed from its original standard value of 20 W m^{-2} K^{-1}. All modes react to a smaller value of λ (which is the way to separate the wave from the overlying atmosphere and recover the ocean-only solution) but only the unstable mode is sensitive to greater values, being the direct consequence of the coupling. Clearly, λ is a necessary condition for the existence of the coupled mode but it is not controlling its growth rate as strongly as the existent stratification. Also, the vertical unstable eigenmodes at different values of λ are not shown, as no significant modifications are found for changes in the air–sea coefficient.

The weak effect of changes in the exchange coefficient was also demonstrated in Huck et al. (2001) when using a vertical diffusivity of 10^{-4} m^2 s^{-1}; in their planetary geostrophic model coupled to an atmospheric EBM they found no dependence of the variability of the system by varying the air–sea exchange coefficient within a range of 10–60 W m^{-2} K^{-1}.

The last parameter subject to study is the vertical diffusivity. The existence of K_v is crucial to the transmission of the information received at the surface to the ocean interior and, although it did not affect the properties of the modes, it is expected to control the behaviour of the unstable mode due to the boundary layer at the top.

In Fig. 10 the solution for different values of K_v is represented (top panels) and the vertical structure of the unstable

[3]For a clear derivation of eqs. (15) and (16) and the relationship between λ and λ_{sa}, λ_{so}, see appendix A in BB98.

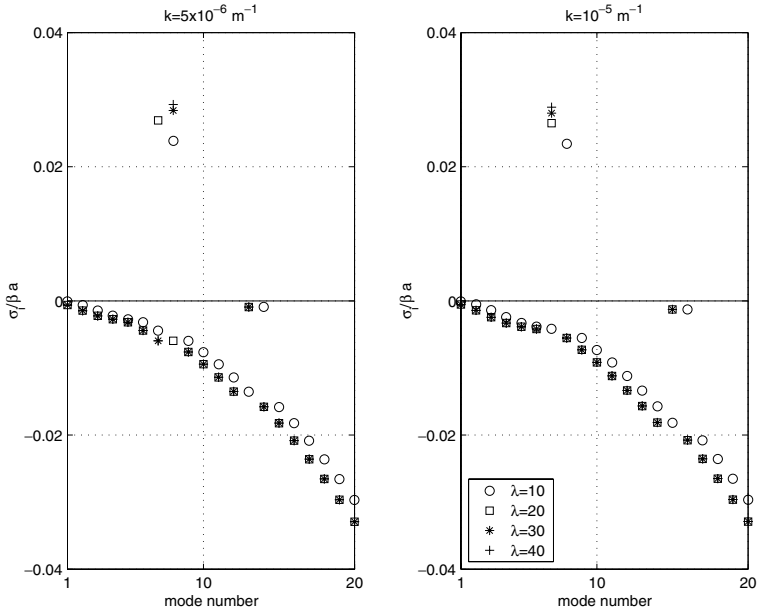

Fig. 9. Same as Fig. 7 for changes in λ. The growing mode responds to an increase or decrease in the air–sea exchange but not dramatically. In contrast, the slowly decaying mode is less affected.

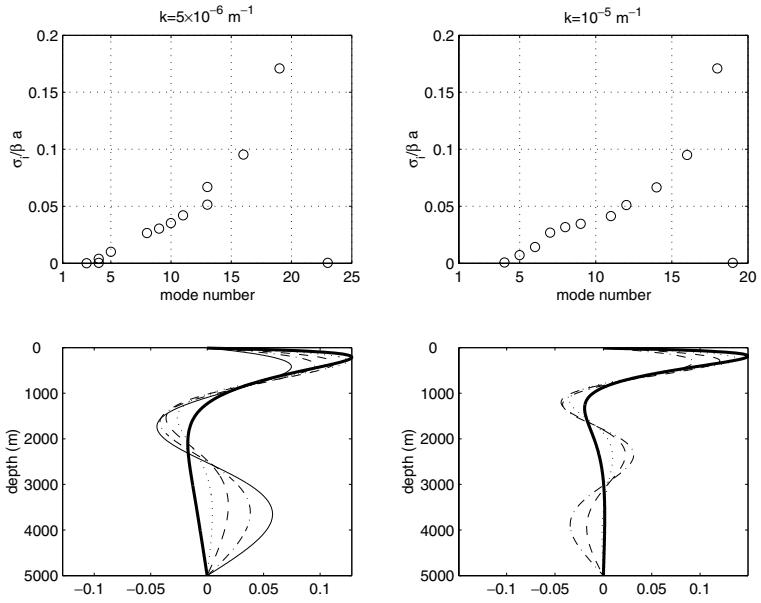

Fig. 10. The dependence of the unstable mode to diffusivity. The position of the mode is shown in the top panels from $K_v = 2 \times 10^{-5}$ (the first value at which the unstable mode appears) to $K_v = 5 \times 10^{-4}$ for $k = 5 \times 10^{-6}$ and $K_v = 4 \times 10^{-4}$ for $k = 10^{-5}$ (the last value of diffusivity supporting the mode). As K_v increases from its critical value, the mode is rapidly destroyed and re-enters the decaying curve of modes. For $k = 5 \times 10^{-6}$ m^{-1} the final position is the third mode and for $k = 10^{-5}$ m^{-1} the fourth mode. This trajectory is reflected in the vertical structure of the bottom panels (thick solid line = $K_v = 10^{-4}$, thin solid line = last vertical structure for which $\sigma_i > 0$).

mode is also given (bottom panels). As diffusivity increases, the unstable mode appears at low mode numbers, reaching its maximum growth for a diffusivity of 3–4 $\times$ 10^{-5} m^2 s^{-1}. Then the growth rate of the unstable mode gradually decreases until it becomes zero for a value of $K_v = 5$–4×10^{-4} m^2 s^{-1} for the two wavelengths considered. While the mode is being destroyed, its vertical structure is slowly modified until it becomes a third or fourth mode, coherent with the frequency trajectory.

The coupled mode, strongly influenced by K_v, is extremely slow with a time-scale of ∼100 yr but has a growth rate of ∼10 yr. This might be interesting in studies concerning climate variability, in which time-scales are of the order of a 100 yr.

Moreover, the unstable mode possesses a vertical structure typical of a first, second or third mode, depending on the wavenumber (Fig. 6). Also, when tested with different values of K_v, it rapidly moved to the fourth and even third position of the eigenspectrum (Fig. 10), adjusting its vertical shape to the modal ordering. What seemed an unimportant mode, far from the first two or three eigenfrequencies, and therefore not likely to play a major role when more complicated physics is added in the ocean, is now a mode that, under certain parameters values, reaches the higher eigenfrequencies and looks like one of them.

This mode could be misleading if identified as a first or second mode and we need to know more about its behaviour. Therefore,

it is interesting to study in detail its time-dependent solution with the help of an initial value problem.

4.2. Time-dependent solution

We here examine briefly the time-dependent solution of the unstable EBM mode. The initial value problem of the damped eigenmodes is not of any particular interest in this case; as predicted by the eigenanalysis, all of them are slowly decaying in time with stronger damping rates for higher modes.

However, the behaviour of the unstable mode during a cycle will inform us about its vertical structure evolution and how its boundary layer grows. The time-dependent problem will also be useful in corroborating the previous numerical solution.

From eqs. (1)–(5) the time-dependent equation reads

$$\left(\partial_t - K_\mathrm{v}\partial_z^2\right) f^2 w_{zz} = \left[(k^2+l^2)\partial_t - \mathrm{i}k\beta\right] N^2 w, \tag{29}$$

which can be rewritten in the condensed form

$$\partial_t \mathcal{L}(w) = \mathcal{M}(w) \tag{30}$$

where the linear operators are $\mathcal{L} = f^2\partial_z^2 - N^2(k^2+l^2)$ and $\mathcal{M} = K_\mathrm{v} f^2 \partial_z^4 - \mathrm{i}k\beta N^2$. The problem was time-stepped using the semi-implicit Crank–Nicholson scheme, which is unconditionally stable and second order in space and time. The initial condition is the solution found with eq. (10) with a different boundary condition at the top for every case and every mode.

The time-stepped EBM involves the system (17)–(18). In our simplified model we neglect the effects of salinity and consider density perturbations driven only by temperature perturbations, i.e. $\rho = -\rho_0 \alpha T$ (where $\alpha = 10^{-4}$ K^{-1} is the coefficient of thermal expansion of sea water). Then the initial conditions can be expressed as (from eq. 9)

$$T_\mathrm{o} = \frac{-\mathrm{i}f^2}{\alpha g(\sigma k^2 + \beta k)} w_{zz} \tag{31}$$

$$T_\mathrm{a} = \lambda_\mathrm{o} T_\mathrm{o} - \Gamma'_\mathrm{o}\partial_z T_\mathrm{o}. \tag{32}$$

and the time-stepped expression for the atmospheric temperature is

$$\partial_t T_\mathrm{a} = \frac{\lambda_\mathrm{sa}}{\gamma_\mathrm{a}} w_{zz}|_\mathrm{top} - \frac{\lambda_\mathrm{sa}+\lambda_\mathrm{a}}{\gamma_\mathrm{a}} T_\mathrm{a}. \tag{33}$$

In order to solve the problem numerically, the integration for T_a is included in the time-stepped matrix system; therefore, the problem $\partial_t w = \mathsf{A}^{-1}\mathsf{B}w$ becomes of the order of $N+1$.

The time-stepped solution of the unstable modes found in the eigenanalysis can be seen in Fig. 11. After two cycles they grow as predicted by their σ_i and so appear more and more surface intensified. In Fig. 12 the growing modes for $k = 5\times10^{-6}$ m^{-1} (top panel) and $k = 10^{-5}$ m^{-1} (bottom panel) with the smallest growing rate are plotted ($K_\mathrm{v} = 4\times10^{-4}$ and $K_\mathrm{v} = 3\times10^{-4}$ m^2 s^{-1}, respectively, for $N_0^2 = 10^{-5}$ s^{-2}) confirming their third and fourth mode vertical structure. Therefore, this growing solution is robust, as a large K_v coefficient is needed to destroy it, even though the stratification is rather weak in this case.

The solution given by this initial value problem proves the existence of an unstable mode, which is travelling very slowly but growing at the decadal period, present for every wavenumber and sustained by the interaction with the atmospheric EBM. However, the reasons for the existence of this mode are still unclear, as is the origin of the energy necessary for its growth. A brief discussion of energetics is given in the next section.

4.3. Energetics

In the simple case of constant N^2, some progress can be made towards identifying the source of the instability. We construct a

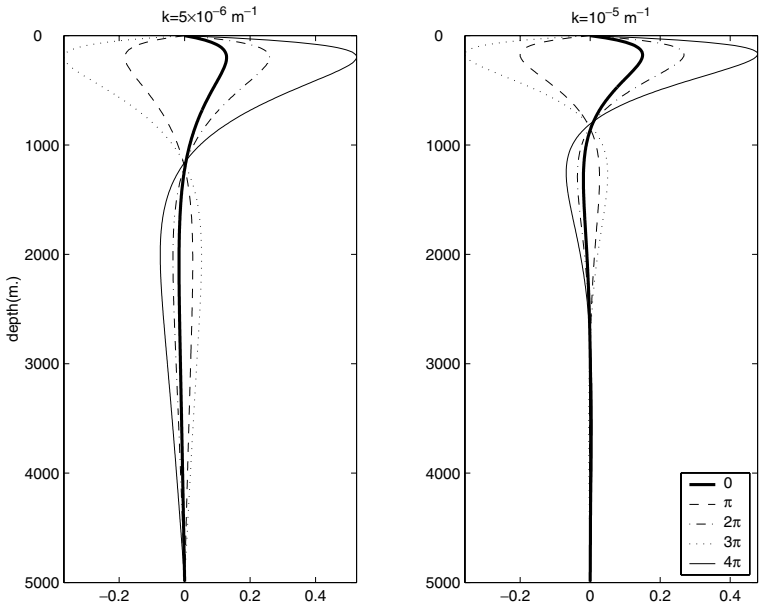

Fig. 11. Time-dependent solution after two cycles for the real part of the growing modes of Fig. 1.

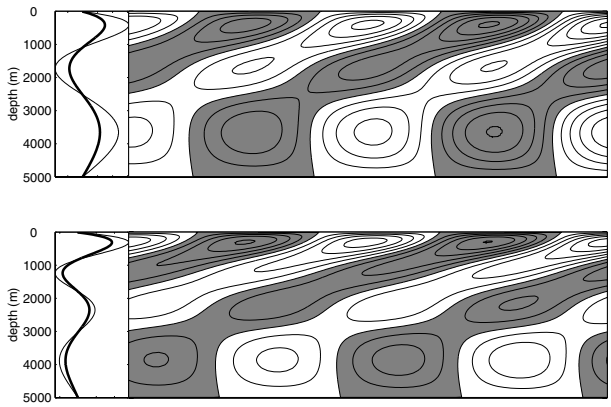

Fig. 12. Time-dependent solution after two cycles for the real part of the slowest growing modes of Fig. 10 (top, $k = 10^{-5}$ m^{-1}; bottom, $k = 5 \times 10^{-6}$ m^{-1}). Left panels: thick line = initial state; thin line = final state. Right panels: evolution of Re(w) during the two cycles integration. The contour interval is 0.025. Negative contours are shaded.

kinetic energy equation by multiplying eqs. (1) and (2) by $\rho_0 u$ and $\rho_0 v$, respectively, adding and integrating over a horizontal wave cycle and depth. To this is added the potential vorticity equation, obtained by multiplying eq. (5) by $g^2\rho/\rho_0 N^2$. The terms in w cancel, leaving

$$E_t \equiv \frac{\partial}{\partial t}\frac{1}{2}\int_{-H}^{0}\left[\rho_0(u^2+v^2)+\frac{g^2\rho^2}{\rho_0 N^2}\right]\mathrm{d}z$$

$$= \frac{K_v g^2}{\rho_0}\int_{-H}^{0}\frac{\rho\rho_{zz}}{N^2}\,\mathrm{d}z. \tag{34}$$

The right-hand side (r.h.s.) cannot be further simplified in general, except when the background stratification is uniform. In that case, integrating by parts,

$$E_t = \frac{K_v g^2}{\rho_0}\left(\left.\frac{\rho\rho_z}{N^2}\right|_{z=0} - \int_{-H}^{0}\frac{\rho_z^2}{N^2}\,\mathrm{d}z\right). \tag{35}$$

The second term is negative definite (the diffusion acting as an energy sink) and the first term can only have a contribution at the surface by eq. (14). In all the cases considered here except the EBM case, the surface contribution is identically zero, and the system energy can only decrease with time, indicating damped solutions.

In the EBM case, however, the potential energy in the EBM atmosphere must also be considered. To obtain this, take eq. (17), with the l.h.s. converted back to $\gamma_a T_{at}$, multiply by λ_{so}, and add λ_{sa} times eq. (18), which eliminates the first terms on the r.h.s., to obtain

$$\gamma_a\lambda_{so}T_aT_{at} + \gamma_o'K_v\lambda_{sa}T_o\,T_{oz}|_{z=0} = -\lambda_{so}(\lambda_{sa}+\lambda_a)T_a^2 + \lambda_{sa}(\lambda_{so}+\lambda_o)T_o^2. \tag{36}$$

Converting ocean temperature to density perturbations through $\rho = -\rho_0\alpha T$, this becomes

$$\frac{\gamma_a\lambda_{so}\rho_0\alpha^2g^2}{\gamma_o'\lambda_{sa}N^2}T_aT_{at} + \frac{K_v g^2}{\rho_0 N^2}\rho\rho_z|_{z=0} = -\frac{\lambda_{so}(\lambda_{sa}+\lambda_a)\rho_0\alpha^2g^2T_a^2}{\gamma_o'\lambda_{sa}N^2} + \frac{(\lambda_{so}+\lambda_o)g^2\rho^2|_{z=0}}{\rho_0\gamma_o'N^2} \tag{37}$$

so that a total energy equation is found by adding eq. (35):

$$E_t + \frac{\gamma_a\lambda_{so}\rho_0\alpha^2g^2}{\gamma_o'\lambda_{sa}N^2}T_aT_{at} = -\frac{K_v g^2}{\rho_0}\int_{-H}^{0}\frac{\rho_z^2}{N^2}\,\mathrm{d}z - \frac{\lambda_{so}(\lambda_{sa}+\lambda_a)\rho_0\alpha^2g^2T_a^2}{\gamma_o'\lambda_{sa}N^2} + \frac{(\lambda_{so}+\lambda_o)g^2\rho^2|_{z=0}}{\rho_0\gamma_o'N^2}. \tag{38}$$

The l.h.s. is a time derivative of a positive definite (quadratic) quantity, and the r.h.s. consists of negative terms apart from the last, which is positive definite. This term, if sufficiently large, can permit growth of the solution as observed.

After performing an eigenanalysis for the case in which the stratification is constant, we use the numerical results to evaluate the three terms in the total energy eq. (38). We are then able to compare the positive term against the other two for the decaying and the growing modes.

In the first mode solution, the negative terms are greater than the positive term indicating a total sink of energy. In the case of the growing mode, the positive term is larger than both decaying terms and the r.h.s. of eq. (38) is positive, confirming an increase in the energy of the system. Also, the energy loss of the decaying modes is much smaller than the energy inputs of the growing modes, confirming again the previous results of growth rates greater than the decaying rates of the first modes.

Moreover, we emphasize the dependence of the first term in eq. (38) upon K_v. Because the first term is the largest of the negative terms, it will play a major role in balancing the energy conservation against the growing term. Therefore, an increase in the vertical diffusivity coefficient is likely to rapidly counteract the third term as previously observed.

These results are summarized in Table 1 where the total energy budgets of the cases depicted in Fig. 10 are shown. Only the first two damped modes and the unstable mode are analysed. The values of the three terms in eq. (38) are given as a percentage of the total budget, being the first two negative contributions and the third a positive contribution. It is clear how the first term (involving vertical diffusivity) and the third term (the positive contribution) are dominating the budget at all parameter values. In the case of decaying (unstable) modes, the diffusivity (positive) term is responsible for the energy of the system. Also, the term allowing growth becomes weaker with stronger stratifications and bigger diffusivities, which is in agreement with the results shown in Figs. 7 and 10. The position of the unstable mode within the damped modes is shifting depending on the parameter values (as pointed out in the parameter sensitivity analysis) and,

Table 1. Energy budget analysis for different wavenumbers k, vertical diffusivity K_v and constant stratification N_0^2. The three terms in eq. (38) are denoted by t1, t2 and t3, respectively. Note that the first two are negative while the third is positive. The values of each term are given as a percentage of the total energy budget. Shown are the first two damped modes and the unstable mode for every case. The position of the unstable mode varies as the parameters in eq. (38) vary and is not directly comparable with the exponential stratification. The values of the parameters are chosen according to Fig. 10; for each wavenumber, we computed the budget for the least growing modes ($k = 5 \times 10^{-6}$: $K_v = 5 \times 10^{-4}$ and $K_v = 4 \times 10^{-4}$; $k = 1 \times 10^{-5}$: $K_v = 4 \times 10^{-4}$ and $K_v = 3 \times 10^{-4}$ for $N_0^2 = 10^{-5}$) and also shown is an example of change in the background stratification ($k = 5 \times 10^{-6}$: $K_v = 4 \times 10^{-4}$ and $N_0^2 = 10^{-4}$; $k = 1 \times 10^{-5}$: $K_v = 3 \times 10^{-4}$ and $N_0^2 = 10^{-5}$)

		$k = 5 \times 10^{-6}$			$k = 1 \times 10^{-5}$		
		$K_v = 5 \times 10^{-4}$	$K_v = 4 \times 10^{-4}$	$N_0^2 = 10^{-4}$	$K_v = 4 \times 10^{-4}$	$K_v = 3 \times 10^{-4}$	$N_0^2 = 10^{-4}$
Mode 1	% t1	97	98	99	98	96	99
	% t2	1	1	1	1	1	1
	% t3	2	1	0	1	3	0
Mode 2	% t1	96	96	99	97	92	97
	% t2	1	1	1	1	2	1
	% t3	3	3	0	2	7	2
Unstable mode	% t1	15	11	26	13	5	28
	% t2	1	1	1	1	1	1
	% t3	84	88	73	86	94	71

because of the uniform stratification, is always located at higher position than in the exponential case, but always present.

4.4. *Effects of atmospheric heat transport*

We have proved that when the EBM is coupled to the planetary geostrophic model the energy balance might be positive, generating an instability and explaining the results of the eigenmode analysis. However, this is not physically correct and therefore there must be a missing term in the energy budget able to counteract those positive contributions from the EBM and give a final damped solution.

So far, we have considered a one-dimensional model, with the spatial dimension represented by a point at mid-latitudes (30°N). BB98 neglect any meridional variability in both atmosphere and ocean, but atmospheric heat transport (AHT) is an important and effective damping of sea surface temperature anomalies (Pierce et al., 1996). We consider here the effects of eddy-diffusive horizontal heat transport in the atmosphere in its usual parametrization

$$\gamma_a \nabla \cdot (\nabla K_T T_a),$$

where again $\gamma_a = \rho_a C_{pa} H_a$ is the atmospheric heat capacity and K_T is the heat transport coefficient. For our model we neglect any meridional dependence in K_T and set it to 10^6 m^2 s^{-1} as suggested by Huck et al. (2001). Fanning and Weaver (1996) points out that the assumption of diffusive transport is valid only for length-scales bigger than 10^6 m, and we therefore set the new meridional wavenumber to its minimum.

Fig. 13 shows the results for the eigenanalysis of the system where the eigenfrequencies for a selected wavenumber are compared with the previous solution without AHT at different values

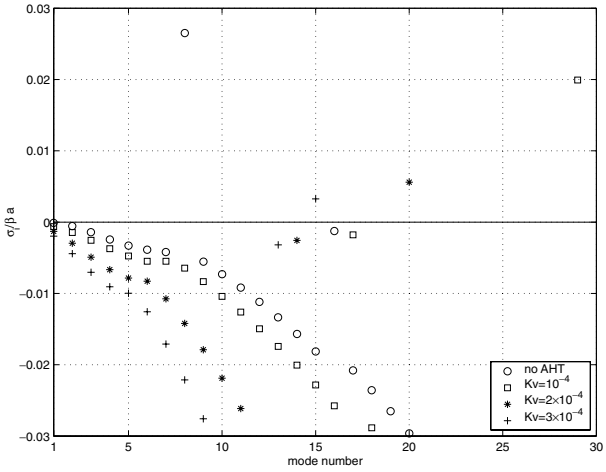

Fig. 13. The effects of the inclusion of horizontal AHT at different vertical diffusivities for $k = 10^{-5}$ m^{-1}. Also plotted is the result with no AHT at $K_v = 10^{-4}$ m^2 s^{-1} (circles).

of vertical diffusion. The additional damping effect is clear for all modes, the unstable mode is weaker and shifted towards higher modes and the effect of K_v in damping the instability is even stronger; however, the growing mode is still present and has the same behaviour as when the AHT is missing. Moreover, calculations with different wavenumbers (both zonal and meridional) did not reveal significant differences. The introduction of horizontal diffusion in the atmosphere will imply an extra term in eq. (23) but this term, together with the second term on the r.h.s., is small compared to the others and therefore does not cause any major modifications in the coupling. Applying eq. (23) with no AHT and also removing the second term show that the ocean

response is not crucially dependent on the term involving the frequency and, in fact, the coupled growing mode maintains a growth rate fairly constant across a wide range of horizontal wavenumbers.

We conclude that, although the AHT is indeed a strong damping mechanism, and together with particular coefficients of diffusivity and stratification can diminish the growth rate, it is not sufficient to balance the positive terms involved in the coupling and further physics should be included in order to compensate the mechanisms generating the unstable mode.

5. Conclusions

In this paper we have examined the behaviour of an oceanic planetary geostrophic model coupled to an atmosphere through an EBM, by examining wave modes with a suitable boundary condition for the vertical velocity in the long-wave limit for a continuously stratified, diffusive, ocean. En route, we have examined the effects on long-wave motions of the diffusivity itself, and several boundary conditions.

The introduction of vertical diffusion has proved to have little effect on the propagation of planetary waves. Qiu et al. (1997) pointed out that the phase speed of the free wave remains unaltered by the inclusion of eddy processes and is also weakly sensitive to changes of its value, but horizontal diffusion can effectively damp the wave. The NF and HF cases are both unable to modify the wave phase speed and also produce small damping rates for the first modes.

The introduction of sensible heat fluxes, and therefore a net loss towards the atmosphere, resulted in only a small increase in the damping rates (Fig. 2, bottom panel). Again, the first three modes seem to remain unchanged. However, this seems to be the more efficient way of damping the planetary wave. When the EBM is introduced, smaller damping rates are found and variations from the unperturbed theory are even less than in the diffusivity case. This is due to the positive contributions of sensible and latent fluxes towards the ocean.

However, when an EBM is used, an additional unstable mode is found. Robust to any change in the parameters, it presents a boundary layer due to the presence of diffusion and a decadal growth rate, but its extremely long period (about 100 yr), while probably irrelevant for decadal processes, is clearly of importance in the interpretation of long climate model runs using a simplified atmosphere. The shape of the unstable mode resemble that of a first mode (no zero crossings in the vertical). This means that the unstable mode found when an atmospheric EBM is coupled to a continuously stratified ocean is not negligible in those parameter settings and could be found with a simpler ocean of fewer layers. Also, its existence has been tested within an initial value problem which proved its growing behaviour.

The sensitivity of the unstable mode to the different parameters taken into account is thoroughly explored. The background stratification has been modified, a homogeneous mixed layer has been included at the surface and a possible range of the coefficient of air–sea exchange λ was used without successfully destroying the instability. Moreover, as K_v seemed to be the main factor in controlling the vertical eigenvectors and growth rate of the unstable mode, we computed the growth rate with a larger range of diffusivity values (Fig. 14) and the unstable mode was found to exist for a relatively wide range of parameter space. When $K_v \to 0$, the ocean and atmosphere stop communicating, or the atmospheric information is not transmitted into the interior ocean; as a result of this, the growing mode cannot exist, and for significant wavelengths, the critical point appears to be at $K_v = 10^{-5}$ m^2 s^{-1}. When K_v reaches its critical value, the bifurcation takes place and the unstable mode appears with a growth rate close to the annual period. Then, as diffusivity increases, the mode is slowly destroyed (as shown in Fig. 10) and its growth rate slows down until it becomes a decaying mode. In fact, the surface intensified disturbance generated by the EBM is rapidly distributed vertically for higher K_v values and the unstable mode no longer exists; this happens for the bottom intensified mode as well.

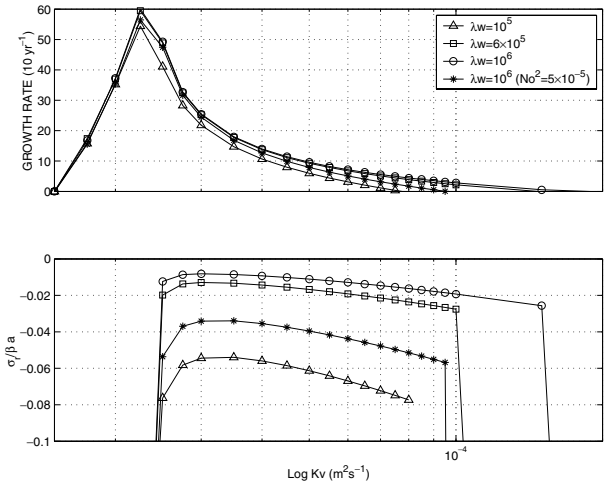

Fig. 14. Semilog plot of the growth rate (top) and Re(σ) (bottom) relation with vertical diffusivity for different wavelengths λ_w (m). When $K_v = 10^{-5}$ m^2 s^{-1} the growing mode appears; its growth rate rapidly increases and then slowly vanishes as K_v approaches values around 10^{-4} m^2 s^{-1} depending on λ_w. For K_v between 4×10^{-5} and 10^{-4} m^2 s^{-1} the growth rate is decadal. Note that for $\lambda_w = 10^6$ m and $N_0^2 = 5 \times 10^{-5}$ s^{-2} (denoted by $*$) also the period of the growing mode is decadal in that region.

It is difficult to give a realistic value for mid-latitude diapycnal diffusivity. Munk and Wunsch (1998), revisiting older studies, concluded that 10^{-4} m^2 s^{-1} is the necessary averaged diffusivity, but other studies using direct estimates at mid-latitudes suggest a lower value of 10^{-5} m^2 s^{-1} (Ledwell et al., 1998). General revisions of the problem (see, for example, Webb and Suginohara, 2001) indicate a range of 3 –5×10^{-5} m^2 s^{-1}.

Within this range, our unstable mode has a decadal growth rate. If we increase the weak stratification to $N_0^2 = 5 \times 10^{-5}$ s^{-2}

and look for waves with $\lambda_w = 10^{-6}$ m, we find a phase speed corresponding to a decadal period (denoted by a star in Fig. 14).

So far, unstable modes in the extratropics have been identified where a dynamical coupling is present in the ocean–atmosphere system (Liu, 1993; Jin, 1997; Frankignoul et al., 1997; Goodman and Marshall, 1999; Talley, 1999; Ferreira et al., 2001), or when the ocean model is coupled to the atmosphere through an EBM with no wind forcing (Huck et al., 2001). However, in this case the instability relied on the zonal background flow to grow, which is not present in our model.

In order to understand the origin of the unstable mode we studied the energetics of the system and identified a positive term that, in the case of the growing mode, is greater than the remaining negative terms and justifies the instability. The simplified atmosphere was improved with the inclusion of horizontal diffusion of heat without achieving a sufficient damping.

It is not clear whether the atmospheric EBM alone could support coupled modes or if this result is an artefact generated by the simplified atmosphere employed, raising doubts over the use of EBMs in coupled studies. Moreover, if dynamics is included in the atmospheric part of the model and the EBM retained, this unstable mode could still be present and possibly confused with a dynamically generated coupled mode.

It might be argued that the use of a constant vertical diffusivity in our ocean could be a lack of representation of the vertical fluxes generated by the EBM, but the results obtained with different N_0^2 and with an explicit mixed layer at the top seem to indicate that the fluxes are not constrained to the top layer but rapidly transmitted to the interior of the ocean, making the use of a constant K_v a reasonable approximation.

However, our model is oversimplified. The lack of dynamics in both the atmosphere and the ocean, horizontal diffusion and meridional boundaries are big limitations in the results obtained in this study. For instance, main flows are key factors for the development of positive ocean–atmosphere feedbacks (Qiu and Jin 1997, for example), meridional boundaries have been proved to cancel the existence of growing modes existing in channel configurations (Goodman and Marshall, 2003). Finally, horizontal diffusion, as discussed by Qiu et al. (1997), although not able to modify the phase speed, is a crucial mechanism for the dissipation of planetary waves and among the primary sinks of energy in the ocean. However, our model is also missing the positive feedback of wind stress, which can reinforce the wave against dissipation, and many studies are based on oversimplified atmospheres or oceans in climate modelling studies, which can result in similar conclusions.

Finally, we conclude that a thermal atmosphere is not efficient in damping out the planetary wave. A dynamic atmosphere needs to be coupled to the planetary wave in order to clarify whether this can be modified in its properties. The unstable mode found when an atmospheric EBM is coupled could disappear but the weakly damped modes could also be excited by wind stress as suggested in recent works (Cessi and Paparella, 2001; Cessi and Primeau, 2001). However, the null negative effects of the thermal atmospheric components leave hope for effective input of energy against any form of dissipation.

6. Acknowledgments

We thank Jeff Blundell for his assistance in the computational part of this study. We also thank an anonymous reviewer and Thierry Huck for their constructive comments that have helped to improve the manuscript. RF acknowledges the support of the University of Southampton under a PhD studentship.

References

Barsugli, J. J. and Battisti, D. S. 1998. The basic effects of atmosphere-ocean thermal coupling on midlatitude variability. *J. Amos. Sci.* **55**, 477–493 (BB98).

Bjornsson, H., Mysak, L. and Schmidt, G. 1997. Mixed boundary conditions versus coupling with an energy-moisture balance model for a zonally averaged ocean climate model. *J. Climate.* **10**, 2412–2430.

Cessi, P. 2000. Thermal feedback on wind stress as a contributing cause of climate variability. *J. Climate* **13**, 232–244.

Cessi, P. and Paparella, F. 2001. Excitation of basin modes by ocean-atmosphere coupling. *Geophys. Res. Lett.* **31**, 3020–3029.

Cessi, P. and Primeau, F. 2001. Dissipative selection of low-frequency modes in a reduced-gravity basin. *J. Phys. Oceanogr.* **31**, 127–137.

Chelton, D. B. and Schlax, M. G. 1996. Global observations of oceanic Rossby waves. *Science* **272**, 234–238.

Colin de Verdière, A. and Blanc, M. L. 2001. Thermal resonance of the atmosphere to SST anomalies. Implications for the Antarctic circumpolar wave. *Tellus* **53A**, 403–424.

Colin de Verdière, A. and Huck, T. 2001. Baroclinic instability: an oceanic wavemaker for interdecadal variability. *J. Phys. Oceanogr.* **29**, 893–910.

Fanning, A. F. and Weaver, A. 1996. An atmospheric energy-moisture balance model: climatology, interpentadal climate change, and coupling to an ocean general circulation model. *J. Geophys. Res.* **101**, 15 111–15 128.

Ferreira, D., Frankignoul, C. and Marshall, J. 2001. Coupled ocean–atmosphere dynamics in a simple mid-latitude climate model. *J. Climate* **14**, 13 704–13 723.

Frankignoul, C., Müller, P. and Zorita, E. 1997. A simple model of decadal response of the ocean to stochastic wind forcing. *J. Phys. Oceanogr.* **27**, 1533–1546.

Gill, A. E. 1982. *Atmosphere–Ocean Dynamics*, Academic Press, International Geophysics Series Vol. 30, 662 pp.

Goodman, J. and Marshall, J. 1999. A model of decadal middle-latitude atmosphere–ocean coupled modes. *J. Climate* **12**, 621–641.

Goodman, J. and Marshall, J. 2003. The role of neutral singular vectors in midlatitude air–sea coupling. *J. Climate* **16**, 88–102.

Haney, R. L. 1971. Surface thermal boundary condition for ocean circulation models. *J. Phys. Oceanogr.* **1**, 241–248.

Harvey, L. D. D. 1988. A semi-analytic energy balance climate model with explicit sea ice and snow physics. *J. Climate* **1**, 1065–1085.

Huck, T. and Vallis, G. K. 2001. Linear stability analysis of the three-dimensional thermally-driven ocean circulation: application to inter-decadal oscillations. *Tellus* **53A**, 526–545.

Huck, T., Vallis, G. K. and Colin de Verdière, A. 2001. On the robustness of the interdecadal modes of the thermohaline circulation. *J. Phys. Oceanogr.* **14**, 940–963.

Jin, F. F. 1997. A theory for interdecadal climate variability of the North Pacific ocean–atmosphere system. *J. Climate* **10**, 1821–1835.

Kiehl, J. T. 1992. Atmospheric general circulation modelling. In: *Climate System Modelling* (ed. K. E. Trenberth), Cambridge University Press, Cambridge, 319–369.

Killworth, P. D. and Blundell, J. R. 1999. The effect of bottom topography on the speed of long extratropical planetary waves. *J. Phys. Oceanogr.* **29**, 2689–2710.

Killworth, P. D. and Blundell, J. R. 2003. Long extratropical planetary wave propagation in the presence of slowly varying mean flow and bottom topography. I: the local problem. *J. Phys. Oceanogr.* **33**, 784–801.

Killworth, P. D., Chelton, D. B. and de Szoeke, R. A. 1997. The speed of observed and theoretical long extratropical planetary waves. *J. Phys. Oceanogr.* **27**, 1946–1966.

Kravtsov, S. and Dewar, W. 2003. On the role of thermohaline advection and sea ice in glacial transitions. *J. Geophys. Res.* **108**, doi:10.1029/2002JC001439.

Ledwell, J., Watson, A. and Law, C. 1998. Mixing of a tracer in the pycnocline. *J. Geophys. Res.* **103**, 21 499–21 529.

Liu, Z. 1993. Interannual positive feedbacks in a simple extratropical air–sea coupling system. *J. Phys. Oceanogr.* **50**, 3022–3028.

Munk, W. and Wunsch, C. 1998. Abyssal recipes II: energetics of tidal and wind mixing. *Deep-Sea Res.* **45**, 1977–2010.

North, G. R. 1975. Theory of energy-balance climate models. *J. Atmos. Sci.* **32**, 2033–2043.

North, G. R., Cahalan, R. F. and Coakley, J. A. 1981. Energy balance climate models. *Rev. Geophys. Space Phys.* **19**, 91–121.

Pierce, D. W., Kim, K-Y. and Barnett, T. P. 1996. Variability of the thermohaline circulation in an ocean general circulation model coupled to an atmospheric energy balance model. *J. Phys. Oceanogr.* **26**, 725–738.

Qiu, B. and Jin, F. F. 1997. Antarctic circumpolar waves: an indication of ocean–atmosphere coupling in the extratropics. *Geophy. Res. Lett.* **24**, 2585–2588.

Qiu, B., Miao, W. and Müller, P. 1997. Propagation and decay of forced and free baroclinic Rossby waves in off-equatorial oceans. *J. Phys. Oceanogr.* **27**, 2405–2417.

Talley, L. 1999. Simple coupled mid-latitude climate models. *J. Phys. Oceanogr.* **29**, 2016–2037.

Trenberth, K. E. (ed.) 1992. *Climate System Modelling*. Cambridge University Press, Cambridge, 788 pp.

Weaver, A. J., Eby, M., Wiebe, E. C., Bitz, C. M., Duffy, P. B. and co-authors. 2001. The UVic Earth System Climate Model: model description, climatology, and applications to past, present and future climates. *Atmos-Ocean* **39**, 361–428.

Webb, D. and Suginohara, N. 2001. Vertical mixing in the ocean. *Nature* **409**, 37.

White, W. B. 2000. Coupled Rossby waves in the Indian ocean on interannual time-scales. *J. Phys. Oceanogr.* **30**, 2972–2988.

White, W. B., Ghao, Y. and Thai, C. K. 1998. Coupling of biennial oceanic Rossby waves with the overlying atmosphere in the Pacific basin. *J. Phys. Oceanogr.* **28**, 1236–1251.